

Flow-based Generative Modeling of Potential Outcomes and Counterfactuals

Dongze Wu and Yao Xie

School of Industrial and Systems Engineering
Georgia Institute of Technology
Atlanta, GA

Email: dwu381@gatech.edu, yao.xie@isye.gatech.edu

David I. Inouye

School of Electrical and Computer Engineering
Purdue University
West Lafayette, IN

Email: dinouye@purdue.edu

Abstract—Predicting potential and counterfactual outcomes from observational data is central to individualized decision-making, particularly in clinical settings where treatment choices must be tailored to each patient rather than guided solely by population averages. We propose PO-Flow, a continuous normalizing flow (CNF) framework for causal inference that jointly models potential outcome distributions and factual-conditioned counterfactual outcomes. Trained via flow matching, PO-Flow provides a unified approach to individualized potential outcome prediction, conditional average treatment effect estimation, and counterfactual prediction. By encoding an observed factual outcome into a shared latent representation and decoding it under an alternative treatment, PO-Flow relates factual and counterfactual realizations at the individual level, rather than generating counterfactuals independently from marginal conditional distributions. In addition, PO-Flow supports likelihood-based evaluation of potential outcomes, enabling uncertainty-aware assessment of predictions. A supporting recovery guarantee is established under certain assumptions, and empirical results on benchmark datasets demonstrate strong performance across a range of causal inference tasks within the potential outcomes framework.

Index Terms—Causal Inference, Counterfactual Prediction, Generative models, Flow-based generative models.

I. INTRODUCTION

Predicting potential outcomes (POs) is central to causal inference and individualized decision-making. In the potential outcomes framework, each individual with covariates X has two outcomes: $Y^{(1)}$ if treated ($A = 1$) and $Y^{(0)}$ if untreated ($A = 0$), but only one factual outcome $Y^{(A)}$ is observed [1]. In applications such as healthcare, practitioners often require patient-level comparisons across treatments, rather than relying solely on population-level averages [2].

Most existing methods focus on estimating the conditional average treatment effect (CATE), $\mathbb{E}[Y^{(1)} - Y^{(0)} | X]$, using meta-learners and model-specific approaches such as representation learning and deep models [3–7]. However, strong CATE performance does not necessarily imply accurate *individualized* potential outcome prediction in finite samples, since the assumptions are sufficient for CATE estimation can be weaker than those required for individual-level modeling [8].

Accurately predicting individualized potential outcomes and learning their conditional distributions $p(Y^{(a)} | X)$ for each treatment $A = a$ is therefore a crucial task, particularly for uncertainty quantification and risk-sensitive decision-making [9]. Recent work has explored generative models for sampling potential outcomes and estimating empirical distributions [10–12]. Nevertheless, methods that learn the full density of potential outcomes within the potential outcomes framework, without relying on restrictive distributional assumptions (e.g., Gaussian mixtures), are still relatively limited in the literature.

Beyond potential outcome prediction, an important but less-studied causal query is *factual-conditioned counterfactual prediction*,

$$Y_{\text{cf}}^{(1-A)} := Y^{(1-A)} | X, Y^{(A)},$$

which asks what would have happened under the alternative treatment, given the observed factual outcome. This differs from standard PO prediction $p(Y^{(A)} | X)$, which does not condition on the realized outcome. Conditioning on $Y^{(A)}$ induces dependence between factual and counterfactual outcomes and is especially relevant for post-hoc analyses (e.g., “would this patient have done better on another therapy?”) [13, 14]. Structural causal models (SCMs) provide a canonical framework for such reasoning, but typically require specifying a causal graph and parametric structural equations [15–17].

In contrast, within the potential outcomes literature, general-purpose methods for individualized *factual-conditioned counterfactual prediction* remain underexplored.¹ This motivates the need for methods that support counterfactual reasoning *without* requiring a parametric SCM, while remaining compatible with the potential outcomes framework.

Despite recent progress, two key gaps remain. First, counterfactual outcome estimation conditioned on the observed factual outcome has received limited attention, despite its importance for individualized and post-hoc

¹Notably, some works [10, 18–20] use the term “counterfactual” to refer to the unobserved potential outcome under an alternative treatment, without conditioning on the observed factual outcome.

analyses. Second, existing methods are often specialized—targeting CATE estimation, potential outcome prediction, or distributional modeling in isolation—rather than providing a unified and scalable framework that jointly addresses these tasks.

In this paper, we propose *PO-Flow*, a continuous normalizing flow (CNF) trained via flow matching [21], which provides a unified generative framework for

- (i) individualized potential outcome prediction,
- (ii) conditional average treatment effect (CATE) estimation,
- (iii) factual-conditioned counterfactual prediction via an abduction–action–prediction procedure enabled by invertible flows, with a supporting recovery result (Corollary V.6), and
- (iv) potential outcome density learning for likelihood-based evaluation and uncertainty quantification.

By encoding an observed factual outcome into a shared latent representation and decoding it under an alternative treatment, PO-Flow enables mapping an individual factual outcome to a corresponding counterfactual outcome at the realization level, rather than generating outcomes independently from marginal conditional distributions.

II. PRELIMINARIES

A Continuous Normalizing Flow (CNF) defines an invertible transformation between a data variable and a simple base variable via a time-dependent Neural Ordinary Differential Equation (ODE). Starting from the data $y(0) = y_0$ at time $t = 0$, the trajectory $y(t)$ evolves according to

$$\frac{dy(t)}{dt} = v_\theta(y(t), t), \quad t \in [0, 1], \quad (1)$$

where $v_\theta : \mathbb{R}^d \times [0, 1] \rightarrow \mathbb{R}^d$ denotes the velocity field parameterized by a neural network with parameters θ .

Under standard regularity conditions, the Neural ODE induces an invertible mapping from the data y_0 at $t = 0$ to a base variable $y_1 = z$ at $t = 1$. The inverse mapping from y_1 to y_0 is obtained by integrating (1) backward in time. Throughout this paper, we adopt the standard choice $y_1 = z \sim \mathcal{N}(0, I)$ at $t = 1$, and denote the corresponding base density by $q(\cdot) = N(0, I)$.

We train the CNF using *conditional flow matching* (CFM) [21, 22], which avoids explicit density simulation. Given a data sample y_0 and an independent base sample $y_1 \sim q(\cdot)$, CFM defines a reference path $\phi_t = \phi(y_0, y_1; t)$ connecting y_0 and y_1 . We adopt the linear interpolant

$$\phi_t = (1 - t)y_0 + ty_1, \quad (2)$$

whose associated reference velocity is

$$\frac{d\phi_t}{dt} = y_1 - y_0. \quad (3)$$

CFM trains the velocity field v_θ to match this reference velocity along the interpolation path by minimizing

$$\begin{aligned} \mathcal{L}_{\text{CFM}}(\theta) \\ = \mathbb{E}_{t \sim \mathcal{U}[0, 1], y_0 \sim p_{\text{data}}, y_1 \sim q(\cdot)} \left\| v_\theta(\phi_t, t) - \frac{d\phi_t}{dt} \right\|^2. \end{aligned} \quad (4)$$

After training, samples are generated by drawing $y_1 \sim q(\cdot)$ and integrating (1) backward in time to obtain y_0 .

III. PROBLEM SETTINGS

In the Potential Outcomes (POs) framework, each individual is characterized by covariates $X \in \mathbb{R}^{d_X}$, a binary treatment assignment $A \in \{0, 1\}$, and an observed factual outcome $Y^{(A)} \in \mathbb{R}$. We observe an i.i.d. dataset

$$\mathcal{D} = \{(y_i, x_i, a_i)\}_{i=1}^n \sim p_{Y, X, A},$$

where $y_i = y_i^{(a_i)}$ denotes the realized potential outcome under the received treatment.

Each individual has two potential outcomes, $Y^{(0)}$ and $Y^{(1)}$, but only one is observed. Potential outcome (PO) prediction targets the conditional distribution $p(Y | X, A = a)$, which equals $p(Y^{(a)} | X)$ under Assumption III.1 when $A = a$. We use $Y^{(a)}$ and $\hat{Y}^{(a)}$ to denote the true and predicted potential outcomes under treatment a , respectively.

The counterfactual outcome asks what would have happened under the *alternative* treatment, given the observed factual outcome $Y^{(a)}$:

$$Y_{\text{cf}}^{(1-a)} := Y^{(1-a)} | X, Y^{(a)}.$$

We denote the true and predicted counterfactual outcomes by $Y_{\text{cf}}^{(1-a)}$ and $\hat{Y}_{\text{cf}}^{(1-a)}$, respectively.

To ensure the identifiability of potential outcomes, we adopt the standard assumptions commonly used in the literature [10, 12, 23]:

- Assumption III.1.**
- 1) *Consistency*: If an individual receives treatment $A = a$, then $Y = Y^{(a)}$.
 - 2) *Unconfoundedness*: All confounders are observed, i.e., $\{Y^{(0)}, Y^{(1)}\} \perp\!\!\!\perp A | X$.
 - 3) *Overlap*: $0 < P(A = 1 | X = x) < 1$ for all $x \in \mathcal{X}$.

Later, we will introduce additional assumptions for factual-conditioned counterfactual prediction in PO-Flow and establish the corresponding theoretical properties.

Algorithm 1: Potential Outcomes Prediction

Require: Trained v_θ

Input: $(x, a) \sim p_{X, A}(\cdot)$

1: $z \sim q(\cdot)$

2: $\hat{y}_0 = z - \int_0^1 v_\theta(y(t), t; x, a) dt$,
with $y(1) = z$.

Return: $\hat{y}^{(a)} := \hat{y}_0$

Algorithm 2: Counterfactual Prediction

Require: Trained v_θ **Input:** Factual sample $(y^{(a)}, x, a) \sim p_{Y,X,A}(\cdot)$

1. Forward process {abduction}:

2. $z = y^{(a)} + \int_0^1 v_\theta(y(t), t; x, a) dt,$
with $y(0) = y^{(a)}$.

3. Reverse process {action and prediction}:

4. Set intervened treatment to $1 - a$;

5. $\hat{y}_0 = z - \int_0^1 v_\theta(y(t), t; x, 1 - a) dt,$
with $y(1) = z$.

Return: $\hat{y}_{\text{cf}}^{(1-a)} := \hat{y}_0$

IV. PROPOSED METHOD

This section presents *PO-Flow*, a continuous normalizing flow framework that jointly supports (i) individualized potential outcome prediction, (ii) factual-conditioned counterfactual prediction, and (iii) learning potential outcome densities.

We model outcomes using a continuous normalizing flow whose velocity field v_θ is conditioned on covariates x and treatment a :

$$\frac{dy(t)}{dt} = v_\theta(y(t), t; x, a), \quad t \in [0, 1]. \quad (5)$$

Given a data point $(y^{(a)}, x, a) \sim p_{Y,X,A}$, we set $y_0 = y^{(a)}$ as the observed training sample at time $t = 0$ and draw a base sample $y_1 = z \sim q(\cdot)$ at $t = 1$.

Under this conditional formulation, the training objective retains the form of conditional flow matching (4) and is given by

$$\mathcal{L}_{\text{CFM}}(\theta) = \mathbb{E}_{\substack{t \sim \mathcal{U}[0,1], \\ (y^{(a)}, x, a) \sim p_{Y,X,A}, \\ y_1 \sim q(\cdot)}} \left\| v_\theta(\phi_t, t; x, a) - \frac{d\phi_t}{dt} \right\|^2, \quad (6)$$

where ϕ_t and $d\phi_t/dt$ are defined in (2) and (3), respectively.

Remark IV.1. Following prior work [23], one may estimate propensity scores $w(x) = p(A = 1 | X = x)$ and apply inverse weighting $1/w(x)$ in the loss. We observed limited empirical improvement and therefore include both weighted and unweighted variants in our implementation.

A. Encoding and Decoding via CNFs

We interpret the forward process as an *encoding* operation, denoted by $Z := \Phi_\theta(Y^{(A)}; X, A)$:

$$z := \Phi_\theta(y^{(a)}; x, a) = y^{(a)} + \int_0^1 v_\theta(y(t), t; x, a) dt, \quad (7)$$

with $y(0) = y^{(a)}$.

Conversely, the reverse process serves as a *decoding* operation:

$$\hat{y}_0 := \Phi_\theta^{-1}(z; x, a) = z - \int_0^1 v_\theta(y(t), t; x, a) dt, \quad (8)$$

with $y(1) = z$.

To generate a *potential outcome* $\hat{y}^{(a)}$ for an individual with (x, a) , we sample $z \sim q(\cdot)$ and decode it using (8). Algorithm 1 summarizes the procedure.

Counterfactual prediction follows an encode–decode procedure. Given a factual sample $(y^{(a)}, x, a)$, the forward process (7) encodes it into z which captures the factual information, and the reverse process (8) then decodes z under the counterfactual treatment $1 - a$ to obtain $\hat{y}_{\text{cf}}^{(1-a)}$. Algorithm 2 summarizes the procedure.

V. THEORETICAL PROPERTIES

We characterize theoretical properties of PO-Flow for (i) factual-conditioned counterfactual recovery under monotone SCMs and (ii) likelihood evaluation for potential outcomes.

A. Counterfactual Recovery under Monotone SCMs

We assume the underlying data-generating process follows a structural causal model (SCM)

$$Y^{(A)} = f_X(A, U),$$

where U denotes exogenous noise. PO-Flow defines an encoding map $Z := \Phi_\theta(Y^{(A)}; X, A)$ via (7).

Assumption V.1. (A1) $U \perp\!\!\!\perp A$.

(A2) For each $A \in \{0, 1\}$, the SCM $f_X(A, U)$ is strictly monotone in U .

(A3) The encoded latent is conditionally treatment-invariant: $Z \perp\!\!\!\perp A | X$.

Remark V.2. In the potential outcomes setting, X is multivariate while the outcome is univariate ($y \in \mathbb{R}$), so (A2) concerns monotonicity in the scalar noise U . It holds automatically under additive SCMs $Y^{(A)} = f_X^*(A) + U$, and can also hold under certain identifiability conditions for nonlinear models [24, 25].

Remark V.3. Assumption (A3) posits that the encoding $Z = \Phi_\theta(Y^{(A)}; X, A)$ is conditionally independent of treatment given X . In the infinite-data limit with exact training, the CNF maps each treatment-conditioned outcome distribution to the same base distribution $q(Z)$, yielding $p_\theta(Z | X, A) = q(Z)$ and (A3) is expected to hold. In finite samples, deviations may arise; we assess this empirically in Appendix D.1 of [26].

Under Assumption V.1, we obtain the following result; see Appendix A of [26] for proofs.

Proposition V.4 (Encoded Z as a function of exogenous noise U). *Let Assumptions III.1 and V.1 hold and assume $U \sim \text{Unif}[0, 1]$. Then there exists a continuously differentiable bijection ψ_X independent of A such that*

$$Z = \Phi_\theta(Y^{(A)}; X, A) = \Phi_\theta(f_X(A, U); X, A) = \psi_X(U).$$

Remark V.5. The assumption $U \sim \text{Unif}[0, 1]$ is without loss of generality: if $Z \sim \mathcal{N}(0, 1)$ with CDF F , then

$U = F(Z) \sim \text{Unif}[0, 1]$, and the SCM can be equivalently written in terms of Z .

Following Proposition V.4, we have the following result on counterfactual recovery under monotone SCMs; see Appendix A of [26] for proofs.

Corollary V.6 (Counterfactual recovery under monotone SCMs). *Assume Assumptions III.1 and V.1 hold. Consider a factual sample $(Y^{(A)}, X, A)$ generated by $Y^{(A)} = f_X(A, U)$ and its encoding $Z = \Phi_\theta(Y^{(A)}; X, A)$. Under the intervention $\text{do}(A = \gamma)$, the true counterfactual is $Y_{\text{cf}}^{(\gamma)} = f_X(\gamma, U)$, and the PO-Flow decoder recovers it almost surely:*

$$\hat{Y}_{\text{cf}}^{(\gamma)} := \Phi_\theta^{-1}(Z; X, \gamma) = Y_{\text{cf}}^{(\gamma)}.$$

B. Likelihood Evaluation for Potential Outcome Densities

PO-Flow also enables explicit likelihood evaluation for potential outcomes via the change-of-variables formula for CNFs; see Appendix A of [26] for the proof.

Proposition V.7. *Given a base sample $z \sim q(\cdot)$ at $t = 1$, the log-density of the decoded outcome at $t = 0$ is*

$$\begin{aligned} & \log p_{\theta, Y|X, A}(y | x, a) \\ &= \log q(z) + \int_0^1 \nabla_y \cdot v_\theta(y(t), t; x, a) dt, \end{aligned} \quad (9)$$

where $y = \Phi_\theta^{-1}(z; x, a)$.

VI. EXPERIMENTS

We compare PO-Flow with model-agnostic mean learners (S-, T-, and DR-learners [3, 27]), representation-based regression (CFR [28]), deep generative methods (CEVAE [19], GANITE [10]), and recent generative baselines based on diffusion (DiffPO [23]) and discrete normalizing flows (INFs [12]). For likelihood-based comparisons, we additionally include Gaussian-process baselines for interventional treatment effects (GP-ITE) [29, 30]. Since counterfactuals and unobserved potential outcomes are unavailable in real-world data, we evaluate on semi-synthetic benchmarks: ACIC 2016/2018, IHDP, and IBM. All results are averaged over 10-fold cross-validation; in all tables, columns I and O denote in-sample (training) and out-of-sample (test) performance, respectively.

We evaluate PO-Flow across five complementary tasks, each designed to assess a distinct capability of the proposed framework. These include (i) point prediction of potential outcomes, (ii) conditional average treatment effect estimation, (iii) learning potential outcome densities for likelihood-based evaluation, (iv) distributional fit of potential outcomes, and (v) factual-conditioned counterfactual outcome prediction. Together, these tasks reflect the core claims of PO-Flow and provide a comprehensive evaluation of its individual-level predictive, distributional, and counterfactual reasoning capabilities.

A. Task 1: Potential Outcome Prediction

We evaluate point prediction of potential outcomes using RMSE using the standard definition $\text{RMSE} = [\frac{1}{n} \sum_{i=1}^n (y_i^{(a)} - \hat{y}_i^{(a)})^2]^{1/2}$. Table I shows that PO-Flow achieves the strongest performance on the majority of datasets.

TABLE I: RMSE of estimated potential outcomes (10-fold cross-validation). Parentheses report standard deviation. I/O denote in-/out-of-sample.

Method	ACIC18		IHDP		IBM	
	I	O	I	O	I	O
PO-Flow	0.53 _(0.10)	0.60 _(0.12)	0.98 _(0.11)	1.19 _(0.13)	0.90 _(0.09)	0.97 _(0.11)
DiffPO	0.52 _(0.13)	0.59 _(0.15)	1.33 _(0.20)	1.40 _(0.22)	1.82 _(0.38)	1.85 _(0.35)
INFs	0.69 _(0.16)	0.78 _(0.17)	1.02 _(0.10)	1.20 _(0.12)	1.52 _(0.24)	1.57 _(0.28)
S-learner	0.54 _(0.09)	0.57 _(0.11)	1.31 _(0.18)	1.44 _(0.20)	1.01 _(0.17)	1.16 _(0.19)
T-learner	1.57 _(0.32)	1.71 _(0.40)	1.45 _(0.25)	1.49 _(0.27)	1.89 _(0.47)	1.96 _(0.50)
CEVAE	0.83 _(0.17)	0.85 _(0.17)	1.18 _(0.15)	1.36 _(0.18)	0.96 _(0.12)	0.98 _(0.12)
CFR	0.94 _(0.10)	0.98 _(0.12)	1.10 _(0.20)	1.18 _(0.20)	2.09 _(0.45)	2.17 _(0.48)
GANITE	0.88 _(0.15)	0.97 _(0.15)	1.60 _(0.36)	1.67 _(0.34)	2.48 _(0.39)	2.59 _(0.47)

B. Task 2: Conditional Average Treatment Effect (CATE)

CATE is defined as $\tau(x) = \mathbb{E}[y^{(1)} - y^{(0)} | X = x]$, representing the expected treatment effect conditioned on covariates x . We evaluate CATE using the precision in estimation of heterogeneous effect (PEHE) [31], defined as:

$$\epsilon_{\text{PEHE}} = \frac{1}{n} \sum_{i=1}^n (\hat{\tau}(x_i) - \tau(x_i))^2, \quad (10)$$

where $\hat{\tau}(x) = \mathbb{E}_{p_\theta(\cdot|x,1)}[Y] - \mathbb{E}_{p_\theta(\cdot|x,0)}[Y]$, approximated by Monte Carlo samples from PO-Flow. Table II reports the root PEHE for training and test sets. PO-Flow achieves the most accurate CATE estimates on most datasets.

TABLE II: Measuring precision in estimation of the heterogeneous effect using $\sqrt{\epsilon_{\text{PEHE}}}$; Standard deviations omitted and they are reasonably small. I/O denote in-/out-of-sample.

Method	ACIC16		ACIC18		IHDP		IBM	
	I	O	I	O	I	O	I	O
PO-Flow	0.76	0.82	0.05	0.07	0.41	0.45	0.04	0.04
DiffPO	0.91	1.12	0.07	0.08	0.79	0.84	0.08	0.09
INFs	1.37	1.42	0.33	0.37	0.90	0.95	0.16	0.18
S-learner	3.81	3.87	0.06	0.07	0.92	0.93	0.06	0.07
T-learner	5.02	5.15	1.21	1.32	1.24	1.31	0.60	0.69
DR-learner	3.04	3.51	0.43	0.57	1.03	1.28	0.12	0.19
CEVAE	2.06	2.31	1.19	1.21	1.41	1.43	0.73	0.75
CFR	2.80	2.74	0.77	0.80	0.73	0.78	1.05	1.08
GANITE	3.02	3.11	0.55	0.60	1.90	2.40	0.77	0.80

C. Task 3: Learning Potential Outcome Densities

PO-Flow supports explicit likelihood evaluation of potential outcomes via Proposition V.7. We evaluate density accuracy using the KL divergence between the learned density $p_{\theta, Y|X, A}(\cdot | x, a)$ and the ground-truth density

$p_{\text{true}}(\cdot | x, a)$. For the semi-synthetic benchmarks, $Y^{(a)} \sim \mathcal{N}(\mu_X(a), 1)$, and we compute

$$\text{KL}\left(\hat{Y}^{(a)} \parallel Y^{(a)}\right) = \mathbb{E}_{\hat{y} \sim p_{\theta, Y|X, A}} \left[\log \frac{p_{\theta, Y|X, A}(\hat{y} | x, a)}{\mathcal{N}(\hat{y}; \mu_X(a), 1)} \right],$$

where $p_{\theta, Y|X, A}$ is evaluated via (9). As shown in Table III, PO-Flow achieves lower KL divergence than GP-ITE and INF on ACIC 2018, IHDP, and IBM.

TABLE III: KL divergence of learned potential outcome densities (10-fold cross-validation). Parentheses indicate standard deviation.

Method	ACIC16	ACIC18	IHDP	IBM
PO-Flow	0.14 (0.04)	0.08 (0.02)	0.09 (0.03)	0.08 (0.03)
INF	0.22(0.09)	0.15(0.06)	0.14(0.07)	0.10(0.04)
GP-ITE	1.73(0.34)	0.73(0.19)	1.42(0.30)	0.68(0.17)

Likelihood evaluation also enables selecting the most likely potential outcomes under the learned density. Table IV reports the RMSE of PO-Flow (MAP), where predictions are chosen by maximizing the log-density.

TABLE IV: RMSE for PO-Flow variants (10-fold cross-validation). I/O denote in-/out-of-sample.

Method	ACIC18		IHDP		IBM	
	I	O	I	O	I	O
PO-Flow	0.53	0.60	0.98	1.19	0.90	0.97
PO-Flow (MAP)	0.42	0.54	0.96	1.05	0.84	0.90

D. Task 4: Distributional Fit of Potential Outcomes

To compare estimated potential outcome distributions across methods, we evaluate empirical distribution fit using the Wasserstein-1 distance, following the standard definition

$$W_1(p_{\theta, Y|X, A}(\cdot | x, a), p_{Y|X, A}(\cdot | x, a)) = \inf_{\gamma \in \Gamma(p_{\theta}, p)} \mathbb{E}_{(\hat{y}, y) \sim \gamma} [\|\hat{y} - y\|_1],$$

where Γ denotes the ‘‘coupling’’: the joint distribution between a pair of random variables, whose marginal distributions match p_{θ} and p respectively. Results are reported in Table V. PO-Flow consistently achieves strong performance, indicating accurate recovery of the full potential outcome distributions.

E. Task 5: Factual-Conditioned Counterfactual Outcome Estimation

We evaluate factual-conditioned counterfactual prediction using RMSE between the predicted counterfactual $\hat{y}_{\text{cf}}^{(1-a)}$ and the ground-truth $y_{\text{cf}}^{(1-a)}$. Results are shown in Table VI, which shows the proposed method achieves the best performance. While DiffPO and GANITE do not natively support counterfactual queries, we adapt them for evaluation. Details are provided in Appendix B.5 of [26].

TABLE V: Wasserstein distances (standard deviations omitted, and they are reasonably small). I/O denote in-/out-of-sample.

Method	ACIC16		ACIC18		IHDP		IBM	
	I	O	I	O	I	O	I	O
PO-Flow	0.36	0.42	0.05	0.12	0.30	0.41	0.33	0.44
DiffPO	0.47	0.51	0.04	0.13	0.80	0.88	0.69	0.75
INFs	0.59	0.67	0.08	0.16	0.32	0.40	0.36	0.45
S-learner	1.01	1.02	0.35	0.49	0.71	0.85	0.46	0.55
T-learner	1.22	1.48	1.04	1.00	0.83	0.92	1.21	1.67
CEVAE	0.62	0.70	0.88	1.02	0.65	0.76	0.38	0.45
CFR	0.68	0.73	0.88	0.90	0.50	0.56	0.92	0.93
GANITE	0.74	0.86	0.89	1.18	0.71	0.82	1.09	1.34

TABLE VI: RMSE of estimated counterfactual outcomes (10-fold cross-validation). DiffPO and GANITE do not natively support this query and are adapted by us for evaluation. I/O denote in-/out-of-sample.

Method	ACIC16		ACIC18		IHDP		IBM	
	I	O	I	O	I	O	I	O
PO-Flow	1.50	1.53	0.04	0.05	1.63	1.69	0.04	0.04
DiffPO	1.77	1.78	0.62	0.65	1.81	1.85	0.62	0.64
GANITE	3.41	3.67	0.68	0.70	2.48	2.72	1.84	2.02

Compared to DiffPO and INFs: PO-Flow supports factual-conditioned counterfactual prediction beyond standard potential-outcome modeling. While DiffPO and INFs primarily model interventional outcome distributions, PO-Flow performs counterfactual inference via an encoding-decoding procedure enabled by a smooth and information-preserving path of continuous normalizing flows. Although both baselines can be adapted to this task, they consistently underperform PO-Flow, likely due to INFs’ restrictive discrete-flow parameterization and DiffPO’s forward noising, which limit preservation of factual information.

VII. CONCLUSIONS

We proposed PO-Flow, a continuous normalizing flow framework for causal inference that models potential outcomes and factual-conditioned counterfactuals within the potential outcomes framework. By mapping an observed factual outcome to a shared latent representation and decoding it under alternative treatments, PO-Flow enables individual-level factual-counterfactual mapping without requiring a parametric structural causal model. This supports individualized ‘‘what-if’’ analysis with likelihood-based uncertainty assessment, and the accompanying theory and experiments show that PO-Flow offers a unified and scalable approach to individualized causal reasoning.

ACKNOWLEDGMENT

The work of D.W. and Y.X. are supported by NSF CMMI-2112533, and the Coca-Cola Foundation.

REFERENCES

- [1] P. W. Holland, "Statistics and causal inference," *Journal of the American statistical Association*, vol. 81, no. 396, pp. 945–960, 1986.
- [2] S. Feuerriegel, D. Frauen, V. Melnychuk, J. Schweisthal, K. Hess, A. Curth, S. Bauer, N. Kilbertus, I. S. Kohane, and M. van der Schaar, "Causal machine learning for predicting treatment outcomes," *Nature Medicine*, vol. 30, no. 4, pp. 958–968, 2024.
- [3] S. R. Künzel, J. S. Sekhon, P. J. Bickel, and B. Yu, "Metalearners for estimating heterogeneous treatment effects using machine learning," *Proceedings of the national academy of sciences*, vol. 116, no. 10, pp. 4156–4165, 2019.
- [4] A. Curth and M. Van der Schaar, "Nonparametric estimation of heterogeneous treatment effects: From theory to learning algorithms," in *International Conference on Artificial Intelligence and Statistics*. PMLR, 2021, pp. 1810–1818.
- [5] —, "On inductive biases for heterogeneous treatment effect estimation," *Advances in Neural Information Processing Systems*, vol. 34, pp. 15 883–15 894, 2021.
- [6] N. Acharki, R. Lugo, A. Bertinello, and J. Garnier, "Comparison of meta-learners for estimating multi-valued treatment heterogeneous effects," in *International conference on machine learning*. PMLR, 2023, pp. 91–132.
- [7] J. Schweisthal, D. Frauen, M. Van Der Schaar, and S. Feuerriegel, "Meta-learners for partially-identified treatment effects across multiple environments," in *Forty-first International Conference on Machine Learning*, 2024.
- [8] D. B. Rubin, "Causal inference using potential outcomes: Design, modeling, decisions," *Journal of the American statistical Association*, vol. 100, no. 469, pp. 322–331, 2005.
- [9] F. D. Johansson, U. Shalit, N. Kallus, and D. Sontag, "Generalization bounds and representation learning for estimation of potential outcomes and causal effects," *Journal of Machine Learning Research*, vol. 23, no. 166, pp. 1–50, 2022.
- [10] J. Yoon, J. Jordon, and M. Van Der Schaar, "Ganite: Estimation of individualized treatment effects using generative adversarial nets," in *International conference on learning representations*, 2018.
- [11] V. Melnychuk, D. Frauen, and S. Feuerriegel, "Causal transformer for estimating counterfactual outcomes," in *International conference on machine learning*. PMLR, 2022, pp. 15 293–15 329.
- [12] —, "Normalizing flows for interventional density estimation," in *International Conference on Machine Learning*. PMLR, 2023, pp. 24 361–24 397.
- [13] Z. Yang, Y. Liu, C. Ouyang, L. Ren, and W. Wen, "Counterfactual can be strong in medical question and answering," *Information Processing & Management*, vol. 60, no. 4, p. 103408, 2023.
- [14] R. Guidotti, "Counterfactual explanations and how to find them: literature review and benchmarking," *Data Mining and Knowledge Discovery*, vol. 38, no. 5, pp. 2770–2824, 2024.
- [15] L. G. Neuberg, "Causality: models, reasoning, and inference, by judea pearl, cambridge university press, 2000," *Econometric Theory*, vol. 19, no. 4, pp. 675–685, 2003.
- [16] S. Bongers, P. Forré, J. Peters, and J. M. Mooij, "Foundations of structural causal models with cycles and latent variables," *The Annals of Statistics*, vol. 49, no. 5, pp. 2885–2915, 2021.
- [17] N. Pawlowski, D. Coelho de Castro, and B. Glocker, "Deep structural causal models for tractable counterfactual inference," *Advances in neural information processing systems*, vol. 33, pp. 857–869, 2020.
- [18] F. Johansson, U. Shalit, and D. Sontag, "Learning representations for counterfactual inference," in *International conference on machine learning*. PMLR, 2016, pp. 3020–3029.
- [19] C. Louizos, U. Shalit, J. M. Mooij, D. Sontag, R. Zemel, and M. Welling, "Causal effect inference with deep latent-variable models," *Advances in neural information processing systems*, vol. 30, 2017.
- [20] L. Lei and E. J. Candès, "Conformal inference of counterfactuals and individual treatment effects," *Journal of the Royal Statistical Society Series B: Statistical Methodology*, vol. 83, no. 5, pp. 911–938, 2021.
- [21] Y. Lipman, R. T. Q. Chen, H. Ben-Hamu, M. Nickel, and M. Le, "Flow matching for generative modeling," in *International Conference on Learning Representations (ICLR)*, 2023.
- [22] M. S. Albergo and E. Vanden-Eijnden, "Building normalizing flows with stochastic interpolants," *arXiv preprint arXiv:2209.15571*, 2022.
- [23] Y. Ma, V. Melnychuk, J. Schweisthal, and S. Feuerriegel, "Diffpo: A causal diffusion model for learning distributions of potential outcomes," in *Advances in Neural Information Processing Systems (NeurIPS)*, 2024.
- [24] K. Zhang and A. Hyvarinen, "On the identifiability of the post-nonlinear causal model," *arXiv preprint arXiv:1205.2599*, 2012.
- [25] E. V. Strobl and T. A. Lasko, "Identifying patient-specific root causes with the heteroscedastic noise model," *Journal of Computational Science*, vol. 72, p. 102099, 2023.
- [26] D. Wu, D. I. Inouye, and Y. Xie, "Flow-based generative modeling of potential outcomes and counterfactuals," *arXiv preprint arXiv:2505.16051*, 2025.
- [27] E. H. Kennedy, "Towards optimal doubly robust estimation of heterogeneous causal effects," *Electronic Journal of Statistics*, vol. 17, no. 2, pp. 3008–3049, 2023.
- [28] U. Shalit, F. D. Johansson, and D. Sontag, "Estimating individual treatment effect: generalization bounds and algorithms," in *International conference on machine learning*. PMLR, 2017, pp. 3076–3085.
- [29] A. M. Alaa and M. Van Der Schaar, "Bayesian inference of individualized treatment effects using multi-task gaussian processes," *Advances in neural information processing systems*, vol. 30, 2017.
- [30] B. Huang, C. Chen, J. Liu, and S. Sivaganisan, "Gpmatch: A bayesian causal inference approach using gaussian process covariance function as a matching tool," *Frontiers in Applied Mathematics and Statistics*, vol. 9, p. 1122114, 2023.
- [31] J. Abrevaya, Y.-C. Hsu, and R. P. Lieli, "Estimating conditional average treatment effects," *Journal of Business & Economic Statistics*, vol. 33, no. 4, pp. 485–505, 2015.
- [32] J. L. Hill, "Bayesian nonparametric modeling for causal inference," *Journal of Computational and Graphical Statistics*, vol. 20, no. 1, pp. 217–240, 2011.
- [33] Y. Shimoni, C. Yanover, E. Karavani, and Y. Goldschmidt, "Benchmarking framework for performance-evaluation of causal inference analysis," *arXiv preprint arXiv:1802.05046*, 2018.
- [34] M. F. Hutchinson, "A stochastic estimator of the trace of the influence matrix for laplacian smoothing splines," *Communications in Statistics-Simulation and Computation*, vol. 18, no. 3, pp. 1059–1076, 1989.
- [35] C. Xu, X. Cheng, and Y. Xie, "Normalizing flow neural networks by jko scheme," *Advances in Neural Information*

Processing Systems, vol. 36, pp. 47 379–47 405, 2023.

- [36] Y. Song, J. Sohl-Dickstein, D. P. Kingma, A. Kumar, S. Ermon, and B. Poole, “Score-based generative modeling through stochastic differential equations,” *arXiv preprint arXiv:2011.13456*, 2020.
- [37] S. Chen, S. Chewi, H. Lee, Y. Li, J. Lu, and A. Salim, “The probability flow ode is provably fast,” *Advances in Neural Information Processing Systems*, vol. 36, pp. 68 552–68 575, 2023.
- [38] J. Song, C. Meng, and S. Ermon, “Denoising diffusion implicit models,” *arXiv preprint arXiv:2010.02502*, 2020.
- [39] A. Nasr-Esfahany, M. Alizadeh, and D. Shah, “Counterfactual identifiability of bijective causal models,” in *International conference on machine learning*. PMLR, 2023, pp. 25 733–25 754.

APPENDIX A
PROOFS

Proposition A.1. Assume that $p(y|x, a) > 0$ for all y and $t \in [0, 1]$. Then, up to a constant independent of θ , the Conditional Flow Matching (CFM) loss and the original Flow Matching (FM) loss are equivalent. Hence,

$$\nabla_{\theta} \mathcal{L}_{FM}(\theta) = \nabla_{\theta} \mathcal{L}_{CFM}(\theta).$$

Proof:

We denote the conditional reference velocity field as $u(y, t, x, a|y_0) = \frac{d\phi}{dt} = (1 - \sigma_{\min})y_1 - y_0$, as defined in (3). We further define the marginal (unconditional) reference velocity field as:

$$u(y, t, x, a) = \int u(y, t, x, a|y_0) \frac{p(y, t, x, a|y_0)p_Y(y_0)}{p(y, t, x, a)} dy_0, \quad (11)$$

where $p(y, t, x, a|y_0)$ and $p(y, t, x, a)$ denote the probability densities induced by $u(y, t, x, a|y_0)$ and $u(y, t, x, a)$, respectively. Next, the original flow matching loss, unconditioned on y_0 , is defined as:

$$\mathcal{L}_{FM} = \mathbb{E}_{t \sim \mathcal{U}[0,1], p_{Y,X,A}(\cdot)} \|v_{\theta}(y, t, x, a) - u(y, t, x, a)\|^2. \quad (12)$$

In the main text, we chose ϕ as the linear interpolant between y_0 and y_1 , which results in a constant reference velocity $\frac{d\phi}{dt}$ independent of t . This leads to the simplified CFM loss presented in Eq. (6). However, the general CFM loss, corresponding to an arbitrary reference velocity field $u(y, t | y_0)$ conditioned on y_0 , is defined as:

$$\mathcal{L}_{CFM} = \mathbb{E}_{t \sim \mathcal{U}[0,1], p_Y(y_0), p_{Y,X,A|Y_0}(\cdot|y_0)} \|v_{\theta}(\cdot) - u(\cdot|y_0)\|^2 \quad (13)$$

Next, we have that:

$$\begin{aligned} \|v_{\theta}(y, t, x, a) - u(y, t, x, a)\|^2 &= \|v_{\theta}(\cdot)\|^2 - 2\langle v_{\theta}(\cdot), u(\cdot) \rangle + \|u(\cdot)\|^2 \\ \|v_{\theta}(y, t, x, a) - u(y, t, x, a|y_0)\|^2 &= \|v_{\theta}(\cdot)\|^2 - 2\langle v_{\theta}(\cdot), u(\cdot|y_0) \rangle + \|u(\cdot|y_0)\|^2. \end{aligned} \quad (14)$$

Besides, the term $\mathbb{E}_{t \sim \mathcal{U}[0,1], p_{Y,X,A}(\cdot)} \|v_{\theta}(\cdot)\|^2$ can be equivalently expressed in conditional form as:

$$\begin{aligned} \mathbb{E}_{t \sim \mathcal{U}[0,1], p_{Y,X,A}(\cdot)} \|v_{\theta}(\cdot)\|^2 &= \int \|v_{\theta}(\cdot)\|^2 p_{Y,X,A}(\cdot) dy dx da dt \\ &= \int \|v_{\theta}(\cdot)\|^2 p_{Y,X,A|Y_0}(\cdot|y_0) p_Y(y_0) dy_0 dy dx da dt \\ &= \mathbb{E}_{t \sim \mathcal{U}[0,1], p_Y(y_0), p_{Y,X,A|Y_0}(\cdot|y_0)} \|v_{\theta}(\cdot)\|^2. \end{aligned} \quad (15)$$

Furthermore, by the law of total expectation, we have:

$$\begin{aligned} \mathbb{E}_{t \sim \mathcal{U}[0,1], p_{Y,X,A}(\cdot)} \langle v_{\theta}(\cdot), u(\cdot) \rangle &= \int \left\langle v_{\theta}(\cdot), \frac{\int u(\cdot|y_0) p_{Y,X,A}(\cdot|y_0) p_Y(y_0) dy_0}{p_{Y,X,A}(\cdot)} \right\rangle p_{Y,X,A}(\cdot) dy dx da dt \\ &= \int \left\langle v_{\theta}(\cdot), \int u(\cdot|y_0) p_{Y,X,A}(\cdot|y_0) p_Y(y_0) dy_0 \right\rangle dy dx da dt \\ &= \int \langle v_{\theta}(\cdot), u(\cdot|y_0) \rangle p_{Y,X,A}(\cdot|y_0) p_Y(y_0) dy_0 dy dx da dt \\ &= \mathbb{E}_{t \sim \mathcal{U}[0,1], p_Y(y_0), p_{Y,X,A|Y_0}(\cdot|y_0)} \langle v_{\theta}(\cdot), u(\cdot|y_0) \rangle. \end{aligned} \quad (16)$$

Finally, because $u(\cdot | y_0)$ does not depend on θ , substituting Eqs. (15) and (16) into Eq. (12) and differentiating with respect to θ yields:

$$\nabla_{\theta} \mathcal{L}_{FM}(\theta) = \nabla_{\theta} \mathcal{L}_{CFM}(\theta). \quad (17)$$

Proposition V.4. (Encoded Z as a function of the exogenous noise U) *Let Assumptions III.1 and V.1 hold. Assume that the exogenous noise $U \sim \text{Unif}[0, 1]$. Then there exists a continuously differentiable bijection function $\psi_X : \mathcal{U} \rightarrow \mathcal{Z}$ that is independent of the treatment assignment A , i.e.,*

$$Z = \Phi_\theta(Y^{(A)}; X, A) = \Phi_\theta(f_X(A, U); X, A) = \psi_X(U) \quad \text{a.s.} \quad (18)$$

Proof. Based on the structural causal model, we have $Y^{(A)} = f_X(A, U)$. We define

$$m_{X,A}(U) := Z = \Phi_\theta(Y^{(A)}; X, A) = \Phi_\theta(f_X(A, U); X, A),$$

as a function that may depend on the treatment A . Therefore, our target becomes proving that $m_{X,A}(U)$ is functionally invariant to A .

By (A3) in Assumption V.1, we have $Z \perp\!\!\!\perp A \mid X$. Therefore,

$$p_{\theta, Z|X,A}(z) = p_{\theta, Z|X}(z). \quad (19)$$

In continuous normalizing flows, Φ_θ is invertible with respect to $Y^{(A)}$ due to the invertibility of the underlying neural ODE. In 1-D, this implies that Φ_θ is monotonic in $Y^{(A)} = f_X(A, U)$. Without loss of generality, we assume that Φ_θ is strictly increasing in f_X .

Moreover, by (A2), since $f_X(\cdot, U)$ is strictly monotone in U . Without loss of generality, we assume strictly increasing. Then it follows by the composition rule that $m_{X,A}(U)$ is strictly increasing in U and hence bijective on $[0, 1]$.

Since $Z = \Phi_\theta(Y^{(A)}; X, A) = m_{X,A}(U)$, we may apply change of variables formula w.r.t. U :

$$p_{\theta, Z|X,A}(z) = p_U(m_{X,A}^{-1}(z)) \left| \frac{d}{dz} m_{X,A}^{-1}(z) \right| = 1 \cdot \frac{d}{dz} m_{X,A}^{-1}(z), \quad (20)$$

where the last equation follows from the uniform distribution of U and the fact that $p_Z > 0$.

Next, by combining (19) and (20), we have:

$$p_{\theta, Z|X,A=1}(z) = \frac{d}{dz} m_{X,1}^{-1}(z) = \frac{d}{dz} m_{X,0}^{-1}(z) = p_{\theta, Z|X,A=0}(z). \quad (21)$$

It follows that:

$$m_{X,A}^{-1}(z) = \int^z \frac{d}{dt} m_{X,A}^{-1}(t) dt = \int^z c(t) dt + c_A, \quad (22)$$

where $c(t) = \frac{d}{dt} m_{X,1}^{-1}(t) = \frac{d}{dt} m_{X,0}^{-1}(t)$ is independent of A , and c_A is a constant for each A .

By re-inverting (22), we have:

$$m_{X,A}(u) = (m_{X,A}^{-1})^{-1}(u) = \left(\underbrace{\int^{\bullet} c(t) dt + c_A}_{:=H(\bullet)} \right)^{-1}(u) = H^{-1}(u - c_A). \quad (23)$$

Since $m_{X,A}$ is a bijection $[0, 1] \rightarrow \text{supp}(Z) = \{z \in \mathbb{R} : p_Z(z) > 0\}$, we have:

$$m_{X,A}(0) = \inf \text{supp}(Z), \quad m_{X,A}(1) = \sup \text{supp}(Z), \quad \text{for both } A. \quad (24)$$

Besides, since the support of Z does not depend on A because of (19), we have that

$$\inf \text{supp}(Z) = m_{X,0}(0) = H^{-1}(-c_0) = H^{-1}(-c_1) = m_{X,1}(0). \quad (25)$$

Therefore, $c_0 = c_1 := c$ is a constant that does not depend on A .

Therefore, we can write

$$\psi_X(U) := H^{-1}(U - c) = m_{X,0}(U) = m_{X,1}(U). \quad (26)$$

As a result, we conclude that

$$Z = \Phi_\theta(Y^{(A)}; X, A) = \psi_X(U) \quad \text{a.s.}, \quad (27)$$

is a function that only depends on the exogenous noise U (and covariates X), and is invariant to the treatment A .

Corollary V.6 (Counterfactual recovery) *Assume the conditions in Assumptions III.1 and V.1 hold. Consider a factual sample $(Y^{(A)}, X, A)$ given by the structural equation $Y^{(A)} = f_X(A, U)$, and let its encoded representation be $Z = \Phi_\theta(Y^{(A)}; X, A)$. Apply the intervention $\text{do}(A = \gamma)$. Assume that the true counterfactual is given by $Y_{\text{CF}}^{(\gamma)} = f_X(\gamma, U)$.*

The decoder then recovers the counterfactual almost surely:

$$\hat{Y}_{\text{CF}}^\gamma := \Phi_\theta^{-1}(Z; X, \gamma) = Y_{\text{CF}}^\gamma. \quad (28)$$

Proof. Due to the deterministic and invertible nature of the continuous normalizing flow when the conditioning input is fixed, we have,

$$\Phi_\theta^{-1}(\Phi_\theta(Y; X, A); X, A) = Y. \quad (29)$$

From Proposition V.4, we have $Z = \Phi_\theta(Y^{(A)}; X, A) = \Phi_\theta(f_X(A, U); X, A) = \psi_X(U)$ does not depend on A . Therefore, fixing U as the same and plugging in $\text{do}(A = \gamma)$, we have:

$$\Phi_\theta(Y^{(A)}; X, A) = \Phi_\theta(f_X(A, U); X, A) = \psi_X(U) = \Phi_\theta(f_X(\gamma, U); X, \gamma) = \Phi_\theta(Y_{\text{CF}}^\gamma; X, \gamma), \quad (30)$$

or more simply,

$$\Phi_\theta(Y^{(A)}; X, A) = \Phi_\theta(Y_{\text{CF}}^\gamma; X, \gamma), \quad (31)$$

we further have,

$$\Phi_\theta^{-1}(\Phi_\theta(Y^{(A)}; X, A); X, \gamma) = \Phi_\theta^{-1}(\Phi_\theta(Y_{\text{CF}}^\gamma; X, \gamma); X, \gamma). \quad (32)$$

Noting that the L.H.S. of (32) is exactly the counterfactual procedures (encoding-decoding) of PO-Flow, and by (29), the R.H.S. of (32) equals Y_{CF}^γ . Therefore,

$$\hat{Y}_{\text{CF}}^\gamma := \Phi_\theta^{-1}(Z; X, \gamma) = Y_{\text{CF}}^\gamma. \quad (33)$$

Proposition V.7. *Given a noise sample $z \sim q(\cdot)$ at $t = 1$, the log-density of the resulting potential outcome at $t = 0$, obtained via PO-Flow, is given by:*

$$\log p_{\theta, Y|X, A}(y | x, a, z) = \log q(z) + \int_0^1 \nabla_y \cdot v_\theta(y(t), t; x, a) dt.$$

Proof:

Samples from Continuous Normalizing Flows (CNFs) evolve according to the following Neural ODE:

$$\frac{dy(t)}{dt} = v_\theta(y(t), t; x, a), \quad t \in [0, 1], \quad (34)$$

which induces a corresponding evolution of the sample density governed by the Liouville continuity equation:

$$\partial_t p_\theta(y, t) + \nabla \cdot (p_\theta(y, t) v_\theta(y, t; x, a)) = 0. \quad (35)$$

Here, $p_\theta(y, t)$ denotes the time-dependent probability density of the samples y .

Next, we have that the dynamics of the density $p_\theta(\cdot)$ governed by the velocity field $v_\theta(y, t, x, a)$ is given by:

$$\frac{d}{dt} \log p_\theta(y(t), t) = \frac{\nabla p_\theta(y(t), t) \cdot \partial_t y(t) + \partial_t p_\theta(y(t), t)}{p_\theta(y(t), t)} \quad (36)$$

$$= \frac{\nabla p_\theta \cdot \partial_t y + \partial_t p_\theta}{p_\theta} \Big|_{(y(t), t)} \quad (37)$$

$$= \frac{\nabla p_\theta \cdot v_\theta - \nabla \cdot (p_\theta v_\theta)}{p_\theta} \Big|_{(y(t), t)} \quad (\text{by (34) and (35)}) \quad (38)$$

$$= \frac{\nabla p_\theta \cdot v_\theta - (\nabla p_\theta \cdot v_\theta + p_\theta \nabla \cdot v_\theta)}{p_\theta} \Big|_{(y(t), t)} \quad (39)$$

$$= -\nabla \cdot v_\theta. \quad (40)$$

Starting from an initial sample $z \sim q(\cdot)$ and integrating from $t = 1$ to $t = 0$, we have:

$$\log p_{\theta, Y|X, A}(y(0) | x, a, z) = \log q(z) + \int_0^1 \nabla_y \cdot v_{\theta}(y(t), t; x, a) dt. \quad (41)$$

Besides, if $q(\cdot)$ is selected as the commonly used $N(0, I)$, we have:

$$\log p_{\theta, Y|X, A}(y(0) | x, a, z) = -\frac{d_Y}{2} \log 2\pi - \frac{1}{2} \|z\|^2 + \int_0^1 \nabla_y \cdot v_{\theta}(y(t), t; x, a) dt. \quad (42)$$

APPENDIX B EXPERIMENTAL DETAILS

A. Synthetic Causal Datasets

Counterfactual outcomes are unobservable in real-world data but can be simulated using synthetic datasets. In our experiments, we evaluate on widely used benchmarks, including the Atlantic Causal Inference Conference datasets (ACIC 2016 and ACIC 2018), the Infant Health and Development Program (IHDP) [19, 32], and the IBM Causal Inference Benchmark [33].

The ACIC 2016 dataset contains 4,802 samples with 82 covariates each ($d_X = 82$), ACIC 2018 has 1,000 samples with 177 covariates, The IHDP dataset includes 747 samples with 25 covariates, and the IBM dataset consists of 1,000 samples with 177 covariates. Each dataset provides three synthetic values per individual: the factual outcome $y^{(a)}$, the assigned treatment a , and the mean potential outcomes under both treatments, μ_0 (for $a = 0$) and μ_1 (for $a = 1$).

Moreover, under the following dataset synthesis assumptions: (1) fully specified outcome model $Y^{(A)} = f(X, A) + \epsilon$; (2) shared noise across treatment arms for each individual; and (3) invertibility of the structural function such that, given X , A , and $Y^{(A)}$, one can solve for ϵ — we can synthesize the counterfactual outcome through the following procedure:

1. **Abduction:** infer the unobserved noise term ϵ' from the factual outcome $Y^{(A)}$, covariates X , and treatment A ;
2. **Action:** intervene by changing the treatment assignment to $1 - A$;
3. **Prediction:** use the inferred noise ϵ' and new treatment to compute the counterfactual outcome via $Y^{(1-A)} = f(X, 1 - A) + \epsilon'$.

All datasets are generated using diverse simulation mechanisms, and we provide the specific versions used along with our code. For example, the IHDP dataset is generated using 25 covariates and a coefficient matrix W , following the data-generating process:

$$\begin{aligned} X &\sim \text{Real-world distribution } p_X(\cdot), \\ A &\sim \text{Real-world Treatment assignment based on } X, \\ Y &= A(X\beta - \omega) + (1 - A) \exp((X + W)\beta) + \epsilon, \quad \epsilon \sim N(0, 1). \end{aligned} \quad (43)$$

where β , W , and ω are parameters defined by the specific simulation setting.

B. Neural Network Structure and Implementation Information

The neural network used in experiments on causal datasets takes as input $y(t)$, x , t , and a . The model is composed of the following components: (1) an outcome embedding layer that projects $y(t)$ to the same dimension as the concatenated (x, a) ; (2) a FiLM layer that applies feature-wise affine transformations to the embedded $y(t)$, conditioned on (x, a) ; (3) two residual blocks, each consisting of a gated two-layer MLP conditioned on (x, a) , with residual averaging and skip connections; and (4) a projection layer that maps the final hidden representation to two velocity vectors v_0 and v_1 , corresponding to treatments 0 and 1.

All experiments are conducted on an A100 GPU with 16 GB of memory. The training time for causal datasets depends on the dataset and batch sizes. For example, training on the ACIC 2018 dataset with a batch size of 256 typically takes 2–4 seconds per epoch. Log-density evaluation involves divergence integration and requires significantly more time than other test metrics.

C. Runge-Kutta numerical integration method

We apply the classical 4th-order Runge-Kutta method to solve the Neural ODE in the forward process of PO-Flow. Given a factual outcome $y^{(a)}$, we aim to compute the latent embedding $z = y(1)$ by integrating the velocity field v_θ from $t = 0$ to $t = 1$, with initial condition $y(0) = y^{(a)}$. Let h denote the step size, and define discrete time steps $t_k = kh$, for $k = 0, 1, \dots, T$, such that $Th = 1$. The update rule at each step is:

$$y(t_{k+1}) = y(t_k) + \frac{h}{6} (k_1 + 2k_2 + 2k_3 + k_4),$$

where

$$\begin{aligned} k_1 &= v_\theta(y(t_k), t_k, x, a), \quad k_2 = v_\theta\left(y(t_k) + \frac{h}{2}k_1, t_k + \frac{h}{2}, x, a\right), \\ k_3 &= v_\theta\left(y(t_k) + \frac{h}{2}k_2, t_k + \frac{h}{2}, x, a\right), \quad k_4 = v_\theta(y(t_k) + hk_3, t_k + h, x, a), \end{aligned}$$

with $y(0) = y^{(a)}$ and $y(1) = z$. This produces a numerically integrated trajectory from the observed sample to its latent representation.

D. Hutchinson trace estimator

The computations of the log-density of the POs involve the calculation of $\nabla \cdot v_k(x, t)$, i.e., the divergence of the velocity field represented by a neural network. This may be computed by brute force using reverse-mode automatic differentiation, which is much slower and less stable in high dimensions.

We can express $\nabla \cdot v_\theta(y, t, x, a) = \mathbb{E}_{\epsilon \sim p(\epsilon)} [\epsilon^T J_v(y)\epsilon]$, where $J_v(y)$ is the Jacobian of $v_\theta(y, t, x, a)$ at y . Given a fixed ϵ , we have $J_v(y)\epsilon = \lim_{\sigma \rightarrow 0} \frac{v_\theta(y + \sigma\epsilon, t, x, a) - v_\theta(y, t, x, a)}{\sigma}$, which is the directional derivative of v_θ along the direction ϵ . Therefore, for a sufficiently small $\sigma > 0$, we can propose the following Hutchinson estimator [34, 35]:

$$\nabla \cdot v_\theta(y(t), t, x, a) \approx \mathbb{E}_{p(\epsilon)} \left[\epsilon \cdot \frac{v_\theta(y(t) + \sigma\epsilon, t, x, a) - v_\theta(y(t), t, x, a)}{\sigma} \right], \quad (44)$$

where $p(\epsilon)$ is a distribution in \mathbb{R}^{d_Y} satisfying $\mathbb{E}[\epsilon] = 0$ and $\text{Cov}(\epsilon) = I$ (e.g., a standard Gaussian). This approximation becomes exact as $\sigma \rightarrow 0$.

E. Adapted Implementation Details for DiffPO and GANITE Counterfactuals

DiffPO was not originally designed for counterfactual tasks. However, since DiffPO uses a diffusion model as its base, we are able to adapt the algorithm to incorporate an "encoding" and "decoding" structure similar to that of PO-Flow. Our adapted implementation of their algorithm for counterfactual estimation is summarized in Algorithm 3.

Algorithm 3: Adapted DiffPO for Counterfactual

Input: $(y^{(a)}, x, a) \sim p_{Y, X, A}(\cdot)$

1: $z_0 \leftarrow y^{(a)}$

2: Forward Process:

3: for $t = 0, \dots, T - 1$:

4: $z_{t+1} \leftarrow \sqrt{\frac{\alpha_{t+1}}{\alpha}} z + f_\theta(z, t | x, a) \left(\sqrt{1 - \alpha_{t+1}} - \sqrt{\frac{\alpha_{t+1}(1 - \alpha)}{\alpha}} \right)$

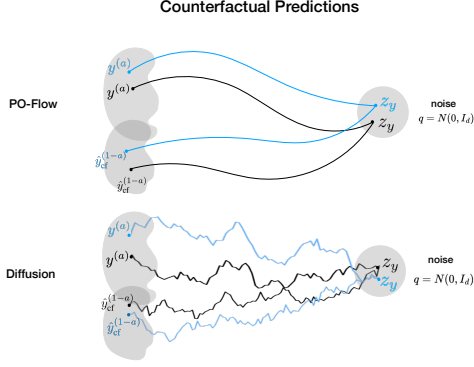
5: $z \leftarrow z_T$

6: Reverse Process:

7: Follow their official implementation in Section 5.3

8: **Return** $\hat{y}^{(1-a)} := \hat{y}_0$

Similarly, GANITE was not originally designed for counterfactual inference. It consists of a generator and a discriminator, with the final output targeting CATE estimation. However, the generator also produces a proxy counterfactual given the factual input, which we use to evaluate its counterfactual estimation performance.



As shown in Figure 1, standard diffusion models use noisy and stochastic forward processes that may degrade the information in z , producing reverse samples that resemble interventional potential outcomes rather than counterfactuals.

In practice, probability flow ODEs [36, 37] or DDIM [38] can be applied to obtain a velocity field equivalent to the ODE derived from the trained diffusion score/noise, under which diffusion and flow matching are theoretically equivalent.

Fig. 1: Illustration of counterfactual predictions. *Left*: two potential outcomes distribution. *Right*: Base (noise) distribution.

APPENDIX C COMPARISONS TO BGM SETTINGS

Bijjective Generation Mechanisms (BGM). The BGM framework [39] shows that if the true structural mechanism f is in the BGM class (bijjective/strictly monotone in the exogenous noise), then any learned mechanism \hat{f} that (i) is also in the BGM class and (ii) *matches the observed distribution*—i.e., for the same parents value X and treatment A ,

$$\hat{f}_X(A, U) \stackrel{d}{=} f_X(A, U) \quad (\text{equivalently } (\hat{f}(X, \cdot))_{\#} P_U = (f(X, \cdot))_{\#} P_U),$$

yields the *same counterfactuals* as f . Their result is model-agnostic, at the class level.

PO-Flow. Our findings are specific to a particular methodology and architecture, as this is a methodology paper where we analyze continuous normalizing flows (CNFs). With the additional assumption (A3) specific to PO-Flow, Proposition V.4 shows that the PO-Flow encoded latent Z is bijjective in the exogenous noise U . Consequently, Corollary V.6 proves that the encode–decode procedure recovers the true counterfactual.

Relationships. Because of Proposition V.4 (enabled by the CNF), PO-Flow implements a bijjective-in-noise mechanism and is thus comparable to BGM in the sense that \hat{f} is bijjective in U . However, BGM additionally requires observational distribution matching to obtain class-level identifiability, whereas the proofs of Proposition V.4 and Corollary V.6 do not assume such matching.

Alternative route. The counterfactual recovery result (Corollary V.6) can alternatively be established by imposing an additional assumption:

(A4) Observational matching. For each (x, a) , the PO-Flow–induced observational law matches the true one, i.e.,

$$(\hat{f}_X(a, \cdot))_{\#} P_U = (f_X(a, \cdot))_{\#} P_U.$$

Under (A1)–(A3), Proposition V.4 establishes a continuously differentiable bijection $\psi_X : U \rightarrow Z$ (independent of A), so the induced mechanism \hat{f}_X implemented by PO-Flow is bijjective in the exogenous noise, i.e., PO-Flow lies in the BGM class. With the additional assumption (A4), we can therefore directly invoke the counterfactual recovery result of the BGM framework [39].

APPENDIX D ADDITIONAL EXPERIMENTAL RESULTS

A. Empirical Validation of Assumption (A3)

We test (A3): $p_{\theta}(Z | X, A) = q(Z) = \mathcal{N}(0, 1)$, using a two-sample Maximum Mean Discrepancy (MMD). Specifically, we test the joint factorization $p(Z, X, A) = q(Z)p(X, A)$ by computing the MMD between the empirical joint sample $\{(z_i, x_i, a_i)\}$ and a synthetic joint sample $\{(z'_i, x_i, a_i)\}$, where $z'_i \sim q = \mathcal{N}(0, 1)$.

We employ a product kernel $k((z, x, a), (z', x', a')) = k_Z(z, z') \cdot k_X(x, x') \cdot k_A(a, a')$, where $k_Z(z, z')$ and $k_X(x, x')$ are radial basis function (RBF) mixtures and $k_A(a, a') = \mathbf{1}[a = a']$ is the indicator kernel for discrete actions:

$$\begin{aligned} k_Z(z, z') &= \exp\left(-\frac{\|z - z'\|^2}{2\sigma_Z^2}\right), \\ k_X(x, x') &= \exp\left(-\frac{\|x - x'\|^2}{2\sigma_X^2}\right). \end{aligned} \quad (45)$$

To set the bandwidths $\{\sigma_Z\}$ and $\{\sigma_X\}$, we first compute the pooled pairwise distances on the union of the observed and synthetic sets (e.g., $\bar{Z} = Z \cup Z'$). We then calculate the median of these distances, and define the bandwidths as $\frac{1}{2}$ median. The empirical MMD is given as:

$$\widehat{\text{MMD}}_u^2 = \frac{1}{n(n-1)} \sum_{i \neq j} k(u_i, u_j) + \frac{1}{n(n-1)} \sum_{i \neq j} k(v_i, v_j) - \frac{2}{n(n-1)} \sum_{i \neq j} k(u_i, v_j), \quad (46)$$

with $u_i = (z_i, x_i, a_i)$, $v_i = (z'_i, x_i, a_i)$.

For more reliable comparisons, we additionally sample two ground-truth sets, $\{(z'_i, x_i, a_i)\}$ and $\{(z''_i, x_i, a_i)\}$, where both $z'_i \sim \mathcal{N}(0, 1)$ and $z''_i \sim \mathcal{N}(0, 1)$. The test is conducted on each dataset considered in the paper, and the aggregated results are summarized in the table below.

TABLE VII: Empirical validation of Assumption (A3), $p_\theta(Z | X, A) = q(Z) = \mathcal{N}(0, 1)$. We report two-sample MMD values comparing the empirical joint distribution $\{(z_i, x_i, a_i)\}$ with synthetic samples $\{(z'_i, x_i, a_i)\}$ across datasets. Lower MMD indicates closer agreement with the assumed factorization $p(Z, X, A) = q(Z)p(X, A)$.

	ACIC 2016	ACIC 2018	IHDP	IBM
PO-Flow	4.9×10^{-2}	7.2×10^{-3}	2.7×10^{-2}	6.8×10^{-2}
True	4.1×10^{-2}	5.9×10^{-3}	2.5×10^{-2}	5.3×10^{-2}

As shown in Table VII, PO-Flow achieves small two-sample joint MMD values, which are comparable to those obtained from the ground-truth independent samples $\{(z'_i, x_i, a_i)\}$ and $\{(z''_i, x_i, a_i)\}$. This provides empirical support for the validity of Assumption (A3).

B. Identifying the Most Likely Potential Outcomes via Log-Density

As shown in Proposition V.7, we can naturally select the most likely potential outcome based on log-density. Table VIII reports the RMSE of PO-Flow when using the most likely PO selected by the algorithm. Specifically, for each sample we simulate 100 POs with PO-Flow, select the one with the highest log-density, and compute the results accordingly.

TABLE VIII: Root mean squared error (RMSE) of estimated potential outcomes (POs) across different methods on the ACIC 2018, IHDP, and IBM datasets. For PO-Flow, results are based on the most likely PO selected from 100 simulated outcomes using log-density. All values are averaged over 10-fold cross-validation.

	ACIC 2018		IHDP		IBM	
	RMSE _{in}	RMSE _{out}	RMSE _{in}	RMSE _{out}	RMSE _{in}	RMSE _{out}
PO-Flow	0.42\pm.07	0.54\pm.10	0.96\pm.09	1.05\pm.10	0.84\pm.06	0.90\pm.08
DiffPO	0.72 \pm .14	0.79 \pm .16	1.33 \pm .20	1.40 \pm .22	1.82 \pm .38	1.85 \pm .35
INFs	0.69 \pm .16	0.78 \pm .17	1.02 \pm .10	1.20 \pm .12	1.52 \pm .24	1.57 \pm .28
S-learner	0.54 \pm .09	0.57 \pm .11	1.31 \pm .18	1.44 \pm .20	1.01 \pm .17	1.16 \pm .19
T-learner	1.57 \pm .32	1.71 \pm .40	1.45 \pm .25	1.49 \pm .27	1.89 \pm .47	1.96 \pm .50
CEVAE	0.83 \pm .17	0.85 \pm .17	1.18 \pm .15	1.36 \pm .18	0.96 \pm .12	0.98 \pm .12
CFR	0.94 \pm .10	0.98 \pm .12	1.10 \pm .20	1.18 \pm .20	2.09 \pm .45	2.17 \pm .48
GANITE	0.88 \pm .15	0.97 \pm .15	1.60 \pm .36	1.67 \pm .34	2.48 \pm .39	2.59 \pm .47

Compared with the averaged RMSE over all POs generated by PO-Flow in Table I, selecting the most likely POs based on log-density yields smaller RMSEs, providing more confident and closer estimates.

C. Convergence and Computational Costs

Figure 2 shows the convergence of RMSE on multiple datasets. PO-Flow demonstrates rapid convergence across datasets, requiring only around 250 training iterations (not epochs) with a batch size of 200 per iteration. This highlights the model's strong training efficiency.

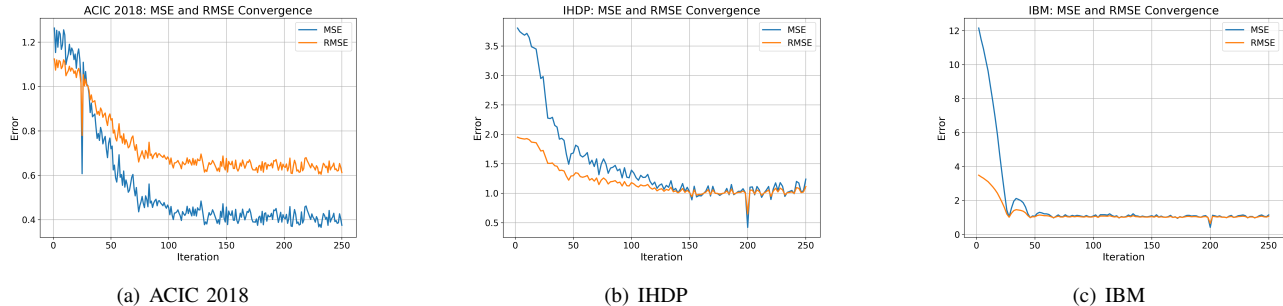


Fig. 2: Convergence of MSE and RMSE for predicted potential outcomes over the training iterations on the ACIC 2018, IHDP, and IBM datasets.

TABLE IX: Comparison of model size, training time until convergence, and sampling cost (for 500 samples).

Methods	# Params	Training Time	Sampling
PO-Flow	32,394	0.96min	0.58s
DiffPO	176,372	5.75min	4.98s
INFs	138,172	5.09min	0.74s
GANITE	167,381	4.93min	0.80s
CEVAE	97,864	4.64min	0.47s

In addition, Table IX compares model size, training time to convergence, and sampling time (for 500 samples) across PO-Flow and other deep generative baselines. All experiments were conducted on a single A100 GPU. Notably, PO-Flow attains superior results with the fewest neural network parameters, leading to faster training and substantially reduced sampling time compared with diffusion-, discrete flow-, and GAN-based methods.